Linear Data Compression of Hyperspectral Images

Kaori Tanji
Chiba University

Hayato Itoh
Nagoya University

Atsushi Imiya
IMIT, Chiba University
imiya@faculty.chiba-u.jp

Naohito Manago
CEReS, Chiba University

Hiroaki Kuze
CEReS, Chiba University

Abstract

The aim of the paper is to analyse hyperspectral images using tensor principal component analysis of multiway data sets. The mathematical and computational backgrounds of pattern recognition are the geometries in Hilbert space for functional analysis and applied linear algebra for numerical analysis, respectively. Because of high-resolution sampling in the colour channels, images observed by a hyperspectral camera system are expressed by three-mode tensors. The Tucker-3 decomposition of a three-mode tensor is used in behaviourmetric science and psychology for the extraction of relations among three entries as an extension of the usual principal component analysis for statistical analysis. Hyperspectral images express spectral information of two-dimensional images on the imaging plane. Therefore, for statistical analysis, we adopt the Tucker-3 decomposition. The Tucker-3 decomposition of hyperspectral images extracts statistically dominant information from hyperspectral images. Tensor principal component analysis allows us to extract dominant light-channel information from hyperspectral images.

1. Introduction

Pattern recognition has played key roles as a mathematical basis for intelligent data processing in modern image science and engineering. We have, over the last decades, witnessed explosive numbers of methods and techniques utilised in pattern recognition. Some of them have been introduced through necessities for applications in industries, businesses, medicine, social security and services and forensics.

In this paper, we propose a statistical method for analysis of hyperspectral images using tensor principal component analysis. Traditionally for multi-colour image analysis, RGB three-channel images are used, since RGB three-channel decomposition is a typical and well-established method for observation and representation for commercial colour image. The RGB three-channel images are measured by observing the reflected light field from observation objects through three filters which produce a triplet of red, green and blue channel images. Furthermore, the image observed by each channel is quantised for representation. These two operations, filtering by three-channel filters and quantisation results in the loss of information in light field reflected from the objects in the space.

On the other hand, hyperspectral cameras measure the reflected light field by decomposing light filed into more than 100 channel-filtered images [1, 2]. Therefore, images observed by such a high-resolution in colour channels preserves more information in the reflected light field than the traditional RGB three-channel cameras. Because of the high sampling rate in colour channels, methods for the extraction of statistically dominant information are desired. Statistically dominant information can be extracted by using principal component analysis (PCA) [3, 4, 5, 6]. Because of high-resolution sampling rate in colour channel, images observed by a hyperspectral camera system are expressed by the three-mode tensors. Therefore, in this paper, we develop a method of PCA for such three-way data expressed in three-mode tensors.

In traditional pattern recognition, sampled patterns for numerical computation are embedded in an appropriate-dimensional Euclidean space as vectors. The other way is to deal with sampled patterns as three-way array data. These three-way array data are expressed as tensors [7, 8, 9, 10, 11, 12] to preserve the linearity of the original pattern space. The subspace method based on the Karhunen-Loève transform is a fundamental technique in pattern recognition. Modern pattern recognition techniques for discretised patterns are described using linear algebra for sampled values embedded in vector space. We express sampled hyperspectral images as three-way array data. These three-way array data are processed as third order tensors. This expression of data requires the development on subspace method for ten-

sor data. For the numerical analysis of the performance e valuation of the proposing algorithm, we have constructed image-database of hyperspectral images.

2. Preliminaries

2.1. PCA in Vector Space

For the orthogonal projections $\boldsymbol{P}$ and $\boldsymbol{P}_\perp = \boldsymbol{I} - \boldsymbol{P}$, $f^\parallel = \boldsymbol{P}f$ and $f^\perp = \boldsymbol{P}_\perp f$ are the canonical element and canonical form of f with respect to $\boldsymbol{P}$ and $\boldsymbol{P}_\perp$, respectively. If $\boldsymbol{P}$ is the projection on to the space spanned by the constant element, the operation $\boldsymbol{P}_\perp f$ is called the constant canonicalisation. Let $\boldsymbol{P}_i$ be the orthogonal projection to the linear subspace corresponding to category C_i. For a pattern f, if $|\boldsymbol{P}_{i^*}(f/|f|)| \leq \delta$ for a sufficiently small positive number δ, we conclude that $f \in C_{i^*}$.

Setting (f, g) to be the inner product in Hilbert space $\mathfrak{H}$, the relation $|f|^2 = (f, f)$ is satisfied. Let θ be the canonical angle between a pair of linear subspaces $\mathfrak{L}_1$ and $\mathfrak{L}_2$. Setting $\boldsymbol{P}_1$ and $\boldsymbol{P}_2$ to be the orthogonal projections to $\mathfrak{L}_1$ and $\mathfrak{L}_2$, respectively, $\cos^2\theta$ is the maximiser of $(\boldsymbol{P}_1 f, \boldsymbol{P}_2 g)^2$ with respect to the conditions $|f| = 1$, $|g| = 1$ $\boldsymbol{P}_1 f = f$ and $\boldsymbol{P}_2 g = g$. The relation $\cos^2\theta = \lambda^2_{\max}$ is satisfied, where $\lambda_{\max}$ is the maximal singular value of $\boldsymbol{P}_2\boldsymbol{P}_1$. Therefore, $\cos^{-1}\lambda_{\max}$ is the principal angle between $\mathfrak{L}_1$ and $\mathfrak{L}_2$. Furthermore, the Grassmann distance between $\mathfrak{L}_1$ and $\mathfrak{L}_2$ is computed by $\sum_{i=1}^{k}\cos^{-1}\lambda_i$.

For f and g in $\mathfrak{H}$, we define the metric d for $\mu(f)$ and $\mu(g)$ such that $d(\mu(f), \mu(g))$ using an appropriate transform μ from $\mathfrak{H}$ to its subset. Furthermore, using an appropriate mapping Φ, we define the measure

$$s(f, g) = \Phi(d(\mu(f), \mu(g))). \tag{1}$$

If we set $\mu(f) = \frac{f}{|f|}$ and set d and Φ as the geodesic distance on the unit sphere in $\mathfrak{H}$ and $\Phi(x) = \cos x$, respectively, $s(f, g)$ becomes a similarity measure based on the angle between f and g. For $f' = f + \delta_f$ and $g' = g + \delta_g$, setting

$$\min(|f|, |g|) = \Lambda, \ \ \max(\delta_f, \delta_g) = \Delta, \tag{2}$$

we have the relation

$$\left|\left(\frac{f'}{|f'|}, \frac{g'}{|g'|}\right) - \left(\frac{f}{|f|}, \frac{g}{|g|}\right)\right| = c\frac{\Delta}{\Lambda}, \tag{3}$$

for a positive constant c. Therefore, $s(f, g)$ is stable and robust against perturbations and noises in f and g.

For patterns in $\mathfrak{H}$, we have the following property.

Property 1 *For $|f| = 1$ and $|g| = 1$, assuming $|f - g| \leq \frac{1}{3}\cdot\frac{\pi}{2}$, the geodesic distance $\theta = d_S(f, g)$ between f and g satisfies the relation $|\theta - |f - g|| < \varepsilon$ for a small positive number ε*

In traditional pattern recognition, sampled patterns are embedded in an appropriate-dimensional Euclidean space as vectors. For $\boldsymbol{x} \in \mathbb{R}^n$ and $\boldsymbol{X} \in \mathbb{R}^{n\times n}$, $|\boldsymbol{x}|_2$ and $|\boldsymbol{X}|_F$ are the vector norm and Frobenius norm of $\boldsymbol{x}$ and $\boldsymbol{X}$, respectively.

Setting the data matrix $\boldsymbol{X}$ to be $\boldsymbol{X} = (\boldsymbol{f}_1, \boldsymbol{f}_2, \cdots, \boldsymbol{f}_m)$ for data vectors $\{\boldsymbol{f}_i\}_{i=1}^m$ in $\mathbb{R}^N$, whose mean is zero, the Karhunen-Loève transform is established by computing $\hat{\boldsymbol{f}}_i = \boldsymbol{U}\boldsymbol{f}_i$ for $\boldsymbol{U}$ which minimises $J_1 = |\boldsymbol{U}\boldsymbol{X}|_F^2$ with the condition $\boldsymbol{U}^\top\boldsymbol{U} = \boldsymbol{I}_N$. The orthogonal matrix $\boldsymbol{U}$ is the minimiser of

$$J_{11} = |\boldsymbol{U}\boldsymbol{X}|_F^2 + \langle(\boldsymbol{U}^\top\boldsymbol{U} - \boldsymbol{I}), \boldsymbol{\Lambda}\rangle, \tag{4}$$

where $\boldsymbol{\Lambda} = Diag(\lambda_1, \lambda_2, \cdots, \lambda_N)$ for $\lambda_1 \geq \lambda_2 \geq \lambda_2 \geq \cdots \geq \lambda_N \geq 0$ and $\langle \boldsymbol{A}, \boldsymbol{B}\rangle = tr\boldsymbol{B}^\top\boldsymbol{A}$. The minimiser of eq. (4) is the solution of the eigenmatrix problem

$$\boldsymbol{M}\boldsymbol{U} = \boldsymbol{U}\boldsymbol{\Lambda}, \ \ \boldsymbol{M} = \boldsymbol{X}\boldsymbol{X}^\top. \tag{5}$$

The row vectors of $\boldsymbol{U}$ are the principal components.

The compression of $\boldsymbol{f}_i$ to a low-dimensional linear subspace is achieved by computing the transform $\boldsymbol{P}_n\boldsymbol{U}\boldsymbol{f}$, where $\boldsymbol{P}_n$, for $n < N$, is the orthogonal projection such that

$$\boldsymbol{P}_n = \begin{pmatrix} \boldsymbol{I}_n & \boldsymbol{O} \\ \boldsymbol{O}^\top & \boldsymbol{O} \end{pmatrix}. \tag{6}$$

2.2. Multispectral and Hyperspectral Images

For a square integrable function $f(\boldsymbol{x})$, which is zero outside of a finite support Ω in three-dimensional Euclidean space, the sample $Sf(\Delta\mathbf{z})$ for $\mathbf{z} \in \mathbf{Z}^2$ and $|\mathbf{z}|_\infty \leq I$ defines an $I \times I$ three-way array $\mathbf{F}$. To preserve the multilinearity of the function $f(\boldsymbol{x})$, we deal with the array $\mathbf{F}$ as a second-order tensor $\mathcal{F}$. The operation $vec\mathcal{F}$ derives a vector $\boldsymbol{f} \in \mathbb{R}^{I_{12}}$ for $I_{12} = I_1 \cdot I_3$. We can reconstruct f from $\mathcal{F}$ using an interpolation procedure.

Setting $\boldsymbol{x} = (x, y)^\top \in \mathbb{R}^2$ and $\mu \geq 0$, a spectral image is expressed as $f(x, y, \mu)$. Grassmann's law of optics and the Young-Helmholtz theory imply that from a colour spectral image $f(\boldsymbol{x}, \mu)$, a three-channel image-triplet is measured as

$$f_i^\alpha(\boldsymbol{x}) = \int_0^\infty w_i^\alpha(\mu) f(\boldsymbol{x}, \mu) d\mu, \ \ i = 1, 2, 3, \tag{7}$$

where α is the label for the selection of channels.

As an extension of Grassmann's law of optics, data acquisition equations for hyperspectral images are mathematically expressed as

$$f(\boldsymbol{x}, k) = \begin{cases} \dfrac{1}{a}\displaystyle\int_{k-\frac{a}{2}}^{k+\frac{a}{2}} f(\boldsymbol{x}, \mu) d\mu, & k > 0, \\ \dfrac{2}{a}\displaystyle\int_0^{\frac{a}{2}} f(\boldsymbol{x}, \mu) d\mu, & k = 0, \end{cases} \tag{8}$$

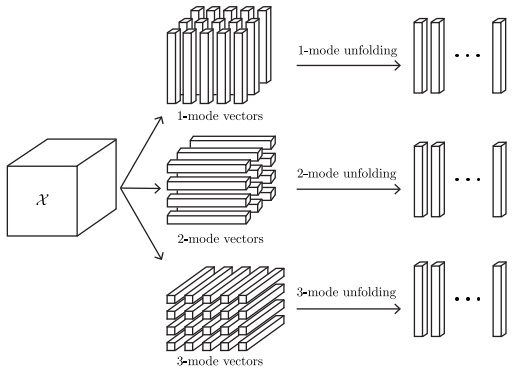

(a) Matrix of images

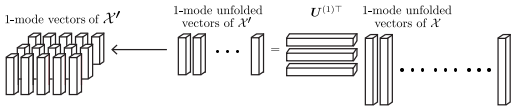

(b) j-mode product

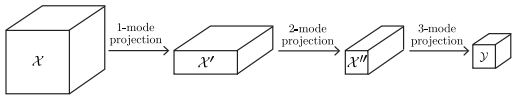

(c) Tensor operation

Figure 1. Tenor expression of hyperspectral images.

where $k - a/2 > 0$. The function $l(\mu;\, k, a)$

$$l(\mu;\, k, a) = \begin{cases} \dfrac{1}{a}, & |\mu - k| \leq \dfrac{a}{2}, \quad k > 0, \\ \dfrac{2}{a}, & 0 \leq \mu \leq \dfrac{a}{2}, \quad k = 0, \end{cases} \tag{9}$$

is the window function for $\mu \geq 0$, which corresponds to $w_i^{\alpha}(\mu)$ in eq. (7).

The sampled image for each channel k is $f_{ijk} = f(\Delta i, \Delta j, k)$, for $(i, j)^{\top} \in \mathbb{Z}^2$, where Δ is a small positive number. Since for all suffices i, j, and k, hyperspectral images are linear, hyperspectral images are elements of the three-mode tenor space $\mathcal{X} \in \mathbb{R}^{m \times n \times l}$.

2.3. Tensor PCA of Hyperspectral Images

For the triplet of positive integers I_1, I_2 and I_3, the third-order tensor $\mathbb{R}^{I_1 \times I_2 \times I_3}$ is expressed as $\mathcal{X} = ((x_{ijk}))$. Indices i, j and k are called the 1-mode, 2-mode and 3-mode of $\mathcal{X}$, respectively. The tensor space $\mathbb{R}^{I_1 \times I_2 \times I_3}$ is interpreted as the Kronecker product of three vector spaces $\mathbb{R}^{I_1}$, $\mathbb{R}^{I_2}$ and $\mathbb{R}^{I_3}$ such that $\mathbb{R}^{I_1} \otimes \mathbb{R}^{I_2} \otimes \mathbb{R}^{I_3}$. We set $I = \max(I_1, I_2, I_3)$. The matrxisation of tensor $\mathcal{X}$ in the mode for $k = 1, 2, 3$ is expressed as

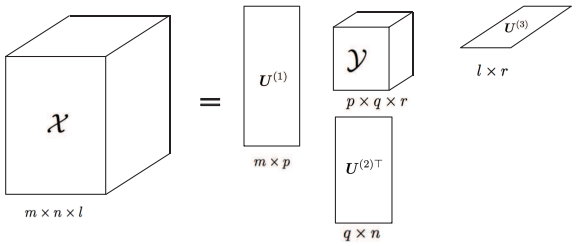

Figure 2. Tensor principal component analysis.

$$\mathcal{X}_{(1)} \in \mathbb{R}^{m \times I_1}, \;\; \mathcal{X}_{(2)} \in \mathbb{R}^{n \times I_2}, \;\; \mathcal{X}_{(3)} \in \mathbb{R}^{l \times I_3}. \tag{10}$$

Then, we have the relations $I_1 = n \times l$, $I_2 = m \times l$ and $I_3 = m \times n$. Figure 1(a) shows an example of matrxisation. Next the j-mode product by $\boldsymbol{U}$ is expressed as

$$\hat{\mathcal{X}}^{(j)} = \mathcal{X} \times_{(j)} \boldsymbol{U}, \; \hat{\mathcal{X}}^{(j)}_{(j)} = \boldsymbol{U}\mathcal{X}_{(j)}. \tag{11}$$

Using orthogonal matrices $\boldsymbol{U}^{(1)}, \boldsymbol{U}^{(2)}, \boldsymbol{U}^{(3)}$, the tensor projection is computed as

$$\mathcal{Y}_i = \mathcal{X} \times_1 \boldsymbol{U}^{(1)\top} \times_2 \boldsymbol{U}^{(2)\top} \times_3 \boldsymbol{U}^{(3)\top} \tag{12}$$

Figure 1(c) shows the geometric operation for the tensor projection. For matrixisation $\mathcal{X}_{(n)}$, the n-mode product is expressed as $\mathcal{X} \times_{(n)} \boldsymbol{U}$. Furthermore, a tensor-to-tensor transformation from is given as

$$\mathcal{Y} = \mathcal{X} \times_1 \boldsymbol{U}^{(1)\top} \times_2 \boldsymbol{U}^{(2)\top} \times_3 \boldsymbol{U}^{(3)\top} \tag{13}$$

For a collection of 3-mode tensors $\{\mathcal{X}_i\}_{i=1}^{N}$, setting the average tensor to be

$$\bar{\mathcal{X}} = \frac{1}{N} \sum_i \mathcal{X}_i, \tag{14}$$

we define

$$\check{\mathcal{X}}_k = \mathcal{X}_k - \bar{\mathcal{X}}. \tag{15}$$

Then, $\boldsymbol{U}^{(j)}$ which mximises the criterion

$$J_3 = \mathop{\mathrm{E}}_{k} \left(|\check{\mathcal{X}}_k \times_1 \boldsymbol{U}^{(1)\top} \times_2 \boldsymbol{U}^{(2)\top} \times_3 \boldsymbol{U}^{(3)\top}|_{\mathrm{F}}^2 \right) \tag{16}$$

with the condition $\boldsymbol{U}^{(j)}\boldsymbol{U}^{(j)\top} = \boldsymbol{I}^{(j)}$. Tensor PCA $\mathcal{Y}$ is computed using $\{\boldsymbol{U}^{(j)}\}_{j=1}^{3}$. Figure 2 shows geometric interpretation of tensor principal component analysis.

The maximisers of eq. (16) is the minimisers of the Euler-Lagrange equation

$$\begin{aligned} & J_{33}(\boldsymbol{U}^{(1)}, \boldsymbol{U}^{(2)}, \boldsymbol{U}^{(3)}) \\ & = \mathop{\mathrm{E}}_{k} \left(|\mathcal{X}_k \times_1 \boldsymbol{U}^{(1)} \times_2 \boldsymbol{U}^{(2)} \times_3 \boldsymbol{U}^{(3)}|_F^2 \right) \\ & + \sum_{i=1}^{3} \langle (\boldsymbol{I} - \boldsymbol{U}^{(i)^{\top}} \boldsymbol{U}^{(i)}), \boldsymbol{\Lambda}^{(i)} \rangle. \end{aligned} \tag{17}$$

This minimisation problem is solved by the following iteration procedure.

1: $\boldsymbol{U}_0^{(i)} := \boldsymbol{Q}^{(i)}$ such that $\boldsymbol{Q}^{(i)\top}\boldsymbol{Q}^{(i)} = \boldsymbol{I}$ and $\alpha = 0$.

2: $\boldsymbol{U}_{(\alpha+1)}^{(1)} = arg\min J_{33}(\boldsymbol{U}^{(1)}, \boldsymbol{U}_{(\alpha)}^{(2)}, \boldsymbol{U}_{(\alpha)}^{(3)})$.

3: $\boldsymbol{U}_{(\alpha+1)}^{(2)} = arg\min J_{33}(\boldsymbol{U}_{(\alpha+1)}^{(1)}, \boldsymbol{U}^{(2)}, \boldsymbol{U}_{(\alpha)}^{(3)})$.

4: $\boldsymbol{U}_{(\alpha+1)}^{(3)} = arg\min J_{33}(\boldsymbol{U}_{(\alpha+1)}^{(1)}, \boldsymbol{U}_{(\alpha+1)}^{(2)}, \boldsymbol{U}^{(3)})$.

5: if $|\boldsymbol{U}_{(\alpha+1)}^{(i)} - \boldsymbol{U}_{(\alpha)}^{(i)}|_F \leq \varepsilon$, then stop, else $\alpha := \alpha + 1$ and go to step 2.

For $J_{33}(\boldsymbol{U}^{(1)}, \boldsymbol{U}^{(2)}, \boldsymbol{U}^{(3)})$, setting $\boldsymbol{U}_1^{(i)} := \boldsymbol{I}$, the system of minimisation problems

$$\begin{aligned} \boldsymbol{U}^{(1)} &= arg\min J_{33}(\boldsymbol{U}^{(1)}, \boldsymbol{I}, \boldsymbol{I}) \\ \boldsymbol{U}^{(2)} &= arg\min J_{33}(\boldsymbol{I}, \boldsymbol{U}^{(2)}, \boldsymbol{I}) \\ \boldsymbol{U}^{(3)} &= arg\min J_{33}(\boldsymbol{I}, \boldsymbol{I}, \boldsymbol{U}^{(3)}) \end{aligned} \tag{18}$$

is derived. This system of minimisation problems derives the following system of eigenmatrix problems,

$$\begin{aligned} \nabla_{\boldsymbol{U}^{(1)}} J_{33}(\boldsymbol{U}^{(1)}, \boldsymbol{I}, \boldsymbol{I}) &= 0 \\ \nabla_{\boldsymbol{U}^{(2)}} J_{33}(\boldsymbol{I}, \boldsymbol{U}^{(2)}, \boldsymbol{I}) &= 0 \\ \nabla_{\boldsymbol{U}^{(3)}} J_{33}(\boldsymbol{I}, \boldsymbol{I}, \boldsymbol{U}^{(3)}) &= 0. \end{aligned} \tag{19}$$

From eq. (19), as an extension of the two-dimensional problem, we define the system of optimisation problems

$$\begin{aligned} J_j &= \mathop{\mathrm{E}}_i \left(|\boldsymbol{U}^{(j)\top} \mathcal{X}_{i,(j)} \boldsymbol{U}^{(j)}|_F^2 \right) \\ &\quad + \langle (\boldsymbol{U}^{(j)\top} \boldsymbol{U}^{(j)} - \boldsymbol{I}_j), \boldsymbol{\Lambda}^{(j)} \rangle \end{aligned} \tag{20}$$

for $j = 1, 2, 3$, as a relaxation of the iteration procedure, where $\mathcal{X}_{i,(j)}$ is the mode j matrixisation of the ith tensor $\mathcal{X}_i$. These optimisation problems derive the system of eigenmatrix problems [13]

$$\boldsymbol{M}^{(j)} \boldsymbol{U}^{(j)} = \boldsymbol{U}^{(j)} \boldsymbol{\Lambda}^{(j)}, \;\; \boldsymbol{M}^{(j)} = \frac{1}{N} \sum_{i=1}^{N} \mathcal{X}_{i,(j)} \mathcal{X}_{i,(j)}^{\top} \tag{21}$$

for $j = 1, 2, 3$.

The eigenvalues of the eigenmatrices in the Tucker-3 orthogonal decomposition satisfy the following theorem.

Theorem 1 *The eigenvalues of* $\boldsymbol{U} = \boldsymbol{U}^{(1)} \otimes \boldsymbol{U}^{(2)} \otimes \boldsymbol{U}^{(3)}$ *define a semi-order.*

(*Proof*) For the eigenvalues $\lambda_i^{(1)}$, $\lambda_j^{(2)}$ and $\lambda_k^{(3)}$ of the 1-, 2- and 3-modes of tensors, respectively, the inequalities

$$\begin{aligned} &\lambda_i^{(1)} \lambda_j^{(2)} \lambda_k^{(3)} \geq \lambda_i^{(1)} \lambda_j^{(2)} \lambda_{k+1}^{(3)}, \\ &\lambda_i^{(1)} \lambda_j^{(2)} \lambda_k^{(3)} \geq \lambda_i^{(1)} \lambda_{j+1}^{(2)} \lambda_k^{(3)}, \\ &\lambda_i^{(1)} \lambda_j^{(2)} \lambda_k^{(3)} \geq \lambda_{i+1}^{(1)} \lambda_j^{(2)} \lambda_k^{(3)}, \end{aligned} \tag{22}$$

define the semi-orders among eigenvalues as

$$\begin{aligned} &\lambda_i^{(1)} \lambda_j^{(2)} \lambda_k^{(3)} \\ &\succeq \left\langle \lambda_i^{(1)} \lambda_j^{(2)} \lambda_{k+1}^{(3)}, \lambda_i^{(1)} \lambda_{j+1}^{(2)} \lambda_k^{(3)}, \lambda_{i+1}^{(1)} \lambda_j^{(2)} \lambda_k^{(3)} \right\rangle. \end{aligned} \tag{23}$$

□

Regarding the selection of the dimension of the tensor subspace, Theorem 1 implies the following theorem.

Theorem 2 *The dimension of the subspace of the tensor space for data compression is* $\frac{1}{6}n(n+1)(n+2)$ *if we select* n *principal components in each mode of three-way array data.*

(*Proof*) For a positive integer n, the number s_n of eigenvalues $\lambda_i^{(1)} \lambda_j^{(2)} \lambda_k^{(3)}$ is

$$\begin{aligned} s_n &= \sum_{i+j+k=0, i,j,k \geq 0}^{n-1} (i+j+k) \\ &= \sum_{l=1}^{n} \sum_{m=1}^{l} m \\ &= \frac{1}{2} \left(\frac{1}{6} n(n+1)(2n+1) + \frac{1}{2} n(n+1) \right) \\ &= \frac{1}{6} n(n+1)(n+2). \end{aligned} \tag{24}$$

□

If $n = 1, 2, 3, 4$, we have $s_n = 1, 4, 10, 20$, respectively, for tensors $\mathcal{X} = ((x_{ijk}))$ in $\mathbb{R}^{I \times I \times I}$.

3. Numerical Examples

The imaging environment is

- GS-A from EBA Japan GS-A and FLD-6II from Toshiba are used as the hyperspectral camera system and light source, respectively.
- GS-A observes spectra from 400nm to 800nm every 5nm using CCD.
- The channel width is 342.125-902.035nm.
- For each pack, 40 images are measured at interval of 9°. Each image is 415×415 pixels and with the colour resolution of 415 channels in colour resolution.

Figures 3(a) and 3 (b) show the configuration of the camera system. Figure 4 illustrates the spectral distribution of light source. Figure 5 shows an example of a data structure for hyperspectral images.

Reconstruction is achieved by selecting leading major components in each mode. The number of major components is same in each mode. From Figure 6 to Figure

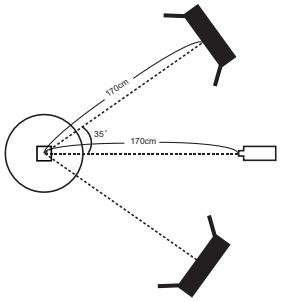

(a) Top view

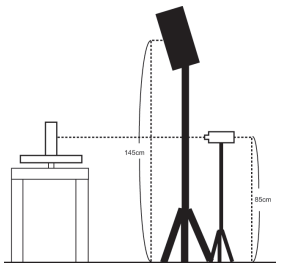

(b) Side wiew

Figure 3. Configuration of the camera and tables

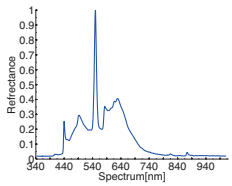

Figure 4. Spectral distribution of light source

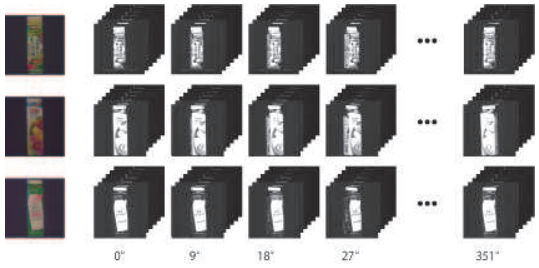

Figure 5. Example of hyperspectral image data.

10, reconstructed images with (a) 4-leading-major, (b) 10-leading-major, (c) 20-leading-major, (d) 35-leading-major, (e) 56-leading-major, (f) 84-leading-major and (g) 415-leading-major principal components are illustrated. Figures 11(a), 11(b) and 11(c) show the cumulative contribution ratio. Figure 11 clarifies that the cumulative contribution ratio depend on the mode.

In our experiments, geometrically rotated images are measured for each image. This observation geometry implies that for reconstruction in the first and second modes, small and large numbers of leading principal components are required, respectively, since in the second mode textures on the images are geometrically deformed by rotation. Furthermore, in the third mode, which expresses the distribution in spectra of images, fewer leading major components are required to reconstruct acceptable images. Furthermore, Figure 11 shows that reconstructions using more than 84 leading major principal components do not posses significant differences. This statistical property of the reconstruction leads to the conclusion that it is possible to reconstruct acceptable hyperspectral images using 0.8% of information in the colour channels.

4. Conclusions

Colour perception of human beings and colour representations for colour images are based on Young-Helmholtz theory, which defines the RGB colour space and filter profiles for three channels of RGB. The RGB colour space is a result of nonlinear data compression from hyperspectral images to three-channel images.

Assuming Grassmann's law for hyperspectral images for recognition, we proposed a statistical method for analysis of hyperspectral images using tensor principal component analysis of multi-way data sets. We have evaluated the validity of the proposing methodology for analysis on hyperspectral images of colour prints, colour paints and natural objects (vegetables). Because of the high sampling rate in colour channels, methods for the extraction of statistically dominant information are desired. This procedure is achieved by using principal component analysis (PCA) for tensors. Images observed by a hyperspectral camera system are expressed by the 3-mode tensors because of high resolution of sampling rate in colour channels. In this paper, assuming that hyperspectral images are three-mode tensors, tensor-based data compression for hyperspectral images is proposed.

The research was supported by "Object oriented data-analysis for understanding and recognition of higher-dimensional multimodal data" by grant for Scientific Research from JSPS, Japan.

References

[1] H.F. Grahn, P. Geladi, *Hyperspectral Image Analysis*, Wiley, 2007.

[2] G. Lua and B. Feia, Medical hyperspectral imaging: a review, Journal of Biomedical Optics, **19**, 010901-(1-23), 2014.

[3] Q. Du, J. E. Fowler, Hyperspectral image compression using JPEG2000 and principal component analysis, IEEE Geoscience and Remote Scensing Letter, **4**, 201-203, 2007.

(a) (b) (c) (d) (e) (f) (g)

Figure 6. Reconstructed images. reconstructions with (a) 4-leading-major, (b) 10-leading-major, (c) 20-leading-major, (d) 35-leading-major, (e)56-leading-major, (f) 84-leading-major and (g) 415-leading-major principal components.

(a) (b) (c) (d) (e) (f) (g)

Figure 7. Reconstructed images. reconstructions with (a) 4-leading-major, (b) 10-leading-major, (c) 20-leading-major, (d) 35-leading-major, (e)56-leading-major, (f) 84-leading-major and (g) 415-leading-major principal components.

[4] J. E. Fowler, Compressive-projection principal component analysis, IEEE TIP, **18**, 2230-2242, 2009.

[5] C. Rodarmel, J. Shan, Principal component analysis for hyperspectral image classification, Surveying and Land Information Systems, **62**, 115-123, 2002.

[6] Q. Du, J. E. Fowler, Low-complexity principal component analysis for hyperspectral image compression, The International Journal of High Performance Computing Applications, **22**, 438-448, 2008.

[7] A. Cichocki, R. Zdunek, A.-H. Phan, S. Amari: *Nonnegative Matrix and Tensor Factorizations: Applications to Exploratory Multi-way Data Analysis and Blind Source Separation*, Wiley, 2009.

[8] M. Itskov: *Tensor Algebra and Tensor Analysis for Engineers*, Springer, 2013.

[9] M. Mørup: Applications of tensor (multiway array) factorizations and decompositions in data mining, Wiley Interdisciplinary Reviews: Data Mining and Knowledge Discovery **1**, 24-40, 2011.

[10] A. Malcev:*Foundations of Linear Algebra*, in Russian edition 1948, (English translation W. H. Freeman and Company, 1963).

[11] T. G. Kolda, B. W. Bader: Tensor decompositions and applications, SIAM Review, **51**, 455-500, 2008.

[12] P. M. Kroonenberg: *Applied Multiway Data Analysis*, Wiley, 2008.

[13] H. Itoh, A. Imiya, T. Sakai, Pattern recognition in multilinear space and its applications: mathematics, computational algorithms and numerical validations, MVA, vol. 27, pp. 1259-1273, 2016.

(a) (b) (c) (d) (e) (f) (g)

Figure 8. Reconstructed images. reconstructions with (a) 4-leading-major, (b) 10-leading-major, (c) 20-leading-major, (d) 35-leading-major, (e)56-leading-major, (f) 84-leading-major and (g) 415-leading-major principal components.

(a) (b) (c) (d) (e) (f) (g)

Figure 9. Reconstructed images. reconstructions with (a) 4-leading-major, (b) 10-leading-major, (c) 20-leading-major, (d) 35-leading-major, (e)56-leading-major, (f) 84-leading-major and (g) 415-leading-major principal components.

(a) (b) (c) (d) (e) (f) (g)

Figure 10. Reconstructed images. reconstructions with (a) 4-leading-major, (b) 10-leading-major, (c) 20-leading-major, (d) 35-leading-major, (e)56-leading-major, (f) 84-leading-major and (g) 415-leading-major principal components.

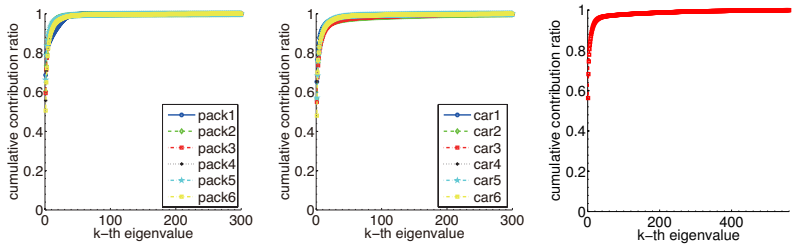

(a) Pack (b) Car (c) Vegetable

Figure 11. Cumulative contribution ratio.